Hanle fluorescence spectra of an atom with a $J_g=0\leftrightarrow J_e=1$ transition

Peng Zhou and S. Swain
Department of Applied Mathematics and Theoretical Physics, The Queen's University of Belfast, Belfast BT7 1NN, United Kingdom
(Received 5 June 1995; revised manuscript received 5 April 1996)

We have investigated the two basic types of Hanle fluorescence spectra, distinguished by the direction of observation, from a V-type atom with a $J_g=0\leftrightarrow J_e=1$ transition excited by a linearly polarized laser. In the absence of a magnetic field to lift the Zeeman degeneracy of the sublevels, the incoherent fluorescence spectrum $G_X^{inc}(\omega)$ is dark for all Rabi frequencies, while the incoherent fluorescence spectrum $G_Y^{inc}(\omega)$ exhibits a single peak for small Rabi frequencies and a Mollow-like triplet for large Rabi frequencies. However, if a magnetic field is applied, the incoherent spectra are composed, in general, of five peaks. When $\omega_B \ll \Omega$, the incoherent spectrum $G_X^{inc}(\omega)$ has four peaks, while $G_Y^{inc}(\omega)$ has a Mollow-like triplet, and the integrated area (i.e., the fluorescence intensity) under the spectrum $G_X^{inc}(\omega)$ is much less than that of $G_Y^{inc}(\omega)$. When $\omega_B \gg \Omega$, both incoherent spectra have a two-peak structure similar to that of a two-level atom far off resonance, but the integrated area under the spectrum $G_X^{inc}(\omega)$ is much greater than that of $G_Y^{inc}(\omega)$. When $\omega_B=\Omega \gg \gamma$, both spectra have a similar five-peak structure, and the same integrated area. The results obtained are interpreted in the dressed atomic state representation. In the strong-field limit, the secular approximation is invoked, and analytical expressions of the resonance fluorescence spectra are derived which demonstrate the dependence of the peak heights and widths of the resonance fluorescence spectra on the intensities of the magnetic and linear polarized laser fields in a more transparent way. [S1050-2947(97)00901-3]

PACS number(s): 42.50.Dv, 32.80.−t, 32.30.−r

I. INTRODUCTION

The Hanle effect [1] is an important phenomenon for investigating the effects of strong coherence on transitions between multilevel atomic states. Its fluorescence radiation exhibits very interesting polarization characteristics due to the interference between the Zeeman sublevels involved in the transition. For a $J_g=0\leftrightarrow J_e=1$ transition, if the linear polarization of the exciting light and the direction of observation are parallel, the observed fluorescence signal is zero at zero magnetic field. When a magnetic field is applied, a nonzero signal is at first obtained, but with an increasing magnetic field, the fluorescence eventually decreases. The effect may be explained in terms of the destructive interference in the angular distribution of atomic radiation from two coherently excited sublevels. A magnetic field reduces the coherence between the excited sublevels through the Zeeman splitting and renders the destructive interference incomplete. Eventually, the magnetic field becomes large enough for the different Zeeman sublevels to be considered uncorrelated.

The Hanle fluorescence signals in the case of monochromatic excitation were investigated theoretically by Avan and Cohen-Tannoudji [2] and observed experimentally at low intensities by Rasmussen, Schieder, and Walther and by Cresser *et al.* [3], where a narrow coherence dip was displayed. The Hanle dip at the zero field broadens with increasing intensity because the stimulated emission and reexcitation partially preserve the coherence between the excited sublevels. On the other hand, the ability of an intense laser to preserve coherence between the $m_J=\pm 1$ excited sublevels depends strongly on the laser bandwidth and statistics. Avan and Cohen-Tannoudji [4] have extended their study of the Hanle signals to the case of a fluctuating intense quasimonochromatic laser beam, and shown that the Hanle fluorescence signals are quite sensitive to fast phase fluctuations. Recently, Arnett *et al.* [5] have carried out an experimental investigation concerning the effect of the laser bandwidth and spectral shape (i.e., the laser coherence properties) on the width and shape of the Hanle dip. Their results showed that when the laser bandwidth increases, power broadening of the Hanle dip normally decreases. A theoretical explanation has also been presented by Ryan and Bergeman [6], who used methods for solving stochastic differential equations [7] to evaluate the Hanle fluorescence signals for the driving laser field with amplitude as well as phase fluctuations. More recently, we have studied the effect of a squeezed vacuum reservoir on the Hanle polarized fluorescence signals [8], and found that the Hanle null does not occur and the Hanle signals are broadened.

Other aspects of the Hanle effect have also been of considerable interest: for example, the fluctuation-induced Hanle resonance in phase conjugation [9], the squeezing of Hanle fluorescence radiation [10], and the mechanical Hanle effect [11] have been reported. For related topics such as fluorescence polarization, alignment and orientation of an atomic state, and level crossing, we refer the reader to the recent special issue of Z. Phys. [12] for comprehensive references.

In the current paper we concentrate on the steady-state incoherent resonance fluorescence spectra of an atomic system with a $J_g=0\leftrightarrow J_e=1$ transition, since this aspect has received little attention in past discussions of the Hanle effect [13]. This study reveals the directional properties of the spectrum. Our organization is as follows. In Sec. II, we present the optical Bloch equations of the Hanle effect. We numerically investigate the Hanle resonance fluorescence spectra in Sec. III, where a large number of features of the incoherent spectra are predicted. In Sec. IV, we have employed the atomic dressed state representation and derived analytical resonance fluorescence spectra under the secular approximation. The agreement with the exact numerical calculations is generally quite satisfactory over the range where

the effective Rabi frequency is sufficiently large. A summary is presented in Sec. V.

II. OPTICAL BLOCH EQUATIONS

We consider an atom, having a ground state with an angular momentum quantum number $J_g=0$ and an excited state with $J_e=1$, with Bohr frequency ω_A, driven by linearly polarized laser light at frequency ω_L. A static magnetic field **B** lifts the degeneracy of the excited Zeeman sublevels, splitting the atomic excited state into three equally spaced sublevels: $|J_e,M_J\rangle=|1,-1\rangle$, $|1,0\rangle$, and $|1,1\rangle$. The splitting ω_B is determined by the amplitude of the magnetic field: $\omega_B=\mu B$, where μ is the gyromagnetic ratio.

The ground-state Zeeman sublevel $|0,0\rangle$ is coupled to the two-excited-state Zeeman sublevels $|1,-1\rangle$ and $|1,+1\rangle$ by the linearly polarized light. (The sublevel $|1,0\rangle$ is not excited and may be ignored in the following.) Hence, we have effectively a V-type system. For simplicity, we abbreviate $|0,0\rangle$, $|1,-1\rangle$ and $|1,+1\rangle$ by $|0\rangle$, $|-\rangle$, and $|+\rangle$, respectively. The atomic level scheme and typical experimental geometry are shown in Fig. 1, where the laser light, polarized linearly along the X axis, propagates along the Y axis, the magnetic field is applied along the Z axis, and they interact with the atomic beam directed along the Z axis. The fluorescence detections are along the X and Y axes, which are, respectively, parallel and perpendicular to the polarization direction of the laser field.

In the frame rotating with the laser frequency ω_L, the Hamiltonian under the rotating-wave approximation (using a system of units in which $\hbar=1$) is of the form

$$H=(\delta+\omega_B)A_{++}+(\delta-\omega_B)A_{--}+[(\Omega_+A_{+0}+\Omega_-A_{-0})e^{i\phi_L}+\text{H.c.}], \tag{1}$$

where $A_{lk}=|l\rangle\langle k|$ represents an energy operator for $l=k$ and a dipole transition operator for $l\neq k$. Here direct transitions between the excited sublevels $|-\rangle$ and $|+\rangle$ are dipole forbidden. The detuning between the atom and the laser field is

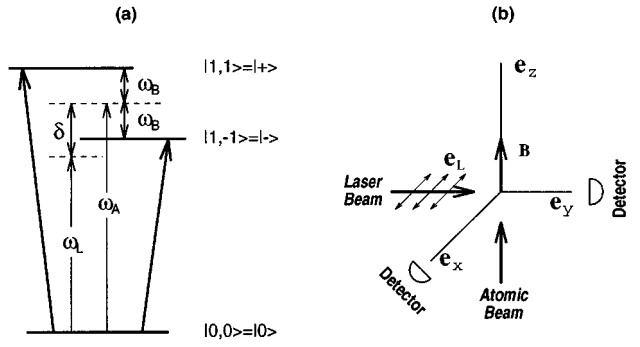

FIG. 1. (a) The atomic level scheme for a $J_g=0\leftrightarrow J_e=1$ transition. (b) The experimental geometry, showing the relative positions of the detectors and beams.

$\delta=\omega_A-\omega_L$. The Rabi frequencies which characterize the atom-laser coupling are given by $\Omega_\pm=E_L\mathbf{e}_L\cdot\mathbf{d}_{\pm0}$, where E_L, ϕ_L, and $\mathbf{e}_L$ are the amplitude, phase, and unit polarization vector (which is taken to lie along $\mathbf{e}_x$) of the laser field, respectively, $\mathbf{d}_{\pm0}$ are the dipole moments for the $|0\rangle\rightarrow|\pm\rangle$ transitions. For the Hanle effect ($J_g=0\leftrightarrow J_e=1$ transition), the vectors $\mathbf{d}_{\pm0}$ are always associated with the σ^+ and σ^- polarizations, respectively. That is, they take the form [6,8,9,14],

$$\mathbf{d}_{-0}=\frac{d}{\sqrt{2}}(\mathbf{e}_x+i\mathbf{e}_y),\quad \mathbf{d}_{+0}=\frac{d}{\sqrt{2}}(\mathbf{e}_x-i\mathbf{e}_y), \tag{2}$$

where the d is the transition amplitudes of two allowed transition pathways. Therefore, for the system considered here $\Omega_+=\Omega_-=\Omega$.

The optical Bloch equation for the system, including the decays of the excited sublevels, is given by [8]

$$\frac{d}{dt}\mathbf{X}(t)=\underline{\mathcal{B}}\mathbf{X}(t)+\mathbf{K}, \tag{3}$$

where the Bloch vector $\mathbf{X}(t)$ is defined as

$$\mathbf{X}(t)=[\langle A_{+0}\rangle,\langle A_{0+}\rangle,\langle A_{++}\rangle,\langle A_{-0}\rangle,\langle A_{0-}\rangle,\langle A_{--}\rangle,\langle A_{+-}\rangle,\langle A_{-+}\rangle]^T. \tag{4}$$

The inhomogeneous term **K** is given by

$$\mathbf{K}=[i\Omega,-i\Omega,0,i\Omega,-i\Omega,0,0,0]^T, \tag{5}$$

and $\underline{\mathcal{B}}$ is the (8×8) matrix

$$\underline{\mathcal{B}}=\begin{bmatrix} -\Lambda_+^* & 0 & -i2\Omega & 0 & 0 & -i\Omega & -i\Omega & 0 \\ 0 & -\Lambda_+ & i2\Omega & 0 & 0 & i\Omega & 0 & i\Omega \\ -i\Omega & i\Omega & -\gamma & 0 & 0 & 0 & 0 & 0 \\ 0 & 0 & -i\Omega & -\Lambda_-^* & 0 & -i2\Omega & 0 & -i\Omega \\ 0 & 0 & i\Omega & 0 & -\Lambda_- & i2\Omega & i\Omega & 0 \\ 0 & 0 & 0 & -i\Omega & i\Omega & -\gamma & 0 & 0 \\ -i\Omega & 0 & 0 & 0 & i\Omega & 0 & -\Lambda_z^* & 0 \\ 0 & i\Omega & 0 & -i\Omega & 0 & 0 & 0 & -\Lambda_z \end{bmatrix}, \tag{6}$$

where

$$\Lambda_{\pm}=\tfrac{1}{2}\gamma+i(\delta\pm\omega_B),\quad \Lambda_z=\gamma+i2\omega_B. \tag{7}$$

The component $\langle A_{ll}\rangle$ in the Bloch vector $\mathbf{X}$ is the population of the level $|l\rangle$, whilst $\langle A_{l0}\rangle$ describes the optical coherence between the excited sublevels $|l\rangle$ and the ground state $|0\rangle$, and $\langle A_{-+}\rangle$ is the Zeeman coherence between the excited sublevels $|+\rangle$ and $|-\rangle$ which develops as a result of the coherent driving of the two allowed transitions. The quantity γ is the decay rate of the excited sublevels to the ground level. The above equation governs the evolution of the system and was employed to study the Hanle polarized fluorescence signals [5,6,8] and nonclassical properties of the Hanle fluorescence radiation [10]. However, we are here interested in the spectral features of the Hanle polarization fluorescence signals, which display remarkable directional properties.

III. HANLE FLUORESCENCE SPECTRA

The fluorescence spectrum is defined in terms of the Fourier transformation of the steady-state correlation between the positive frequency field and the negative frequency field in the far zone

$$G(\omega)=\mathrm{Re}\int_0^\infty\langle\mathbf{E}^{(-)}(\mathbf{r},\tau)\cdot\mathbf{E}^{(+)}(\mathbf{r},0)\rangle e^{-i\omega\tau}d\tau, \tag{8}$$

where the negative frequency part of the radiation field $\mathbf{E}^{(-)}(\mathbf{r},t)$, at a point $\mathbf{r}$ in the far radiation zone takes the form

$$\mathbf{E}^{(-)}(\mathbf{r},t)=\mathbf{E}^{(-)}_{\mathrm{free}}(\mathbf{r},t)-\psi(\mathbf{r})\mathbf{n}\left[\mathbf{n}\times\mathbf{D}^{(+)}\left(t-\frac{r}{c}\right)\right], \tag{9}$$

with $\mathbf{E}^{(-)}_{\mathrm{free}}(\mathbf{r},t)$ being the negative frequency part of the free field operator, $\psi(\mathbf{r})$ a geometrical factor, $\mathbf{n}\equiv\mathbf{r}/r$ a unit vector in the direction of observation, and $\mathbf{D}^{(+)}(t)$ the atomic polarization operator, defined as

$$\mathbf{D}^{(+)}(t)=\mathbf{d}_{+0}A_{+0}(t)+\mathbf{d}_{-0}A_{-0}(t). \tag{10}$$

Hence the steady-state fluorescence spectrum can be expressed in terms of the atomic correlation function

$$G(\omega)=\mathrm{Re}\int_0^\infty\langle\mathbf{n}\times[\mathbf{n}\times\mathbf{D}^{(+)}(\tau)]\cdot\mathbf{n}\times[\mathbf{n}\times\mathbf{D}^{(-)}(0)]\rangle \times e^{-i\omega\tau}d\tau, \tag{11}$$

where $\mathbf{D}^{(-)}(t)=[\mathbf{D}^{(+)}(t)]^*$. It is evident that the fluorescence spectrum is dependent on the direction of observation $\mathbf{n}$. For the $J_g=0\leftrightarrow J_e=1$ transition, the $\mathbf{d}_{\pm0}$ are governed by Eq. (2), and we may reexpress $\mathbf{D}^{(+)}(t)$ as

$$\mathbf{D}^{(+)}(t)=\frac{1}{\sqrt{2}}[D_x^\dagger(t)\mathbf{e}_x+D_y^\dagger(t)\mathbf{e}_y], \tag{12}$$

where

$$D_x^\dagger(t)=d[A_{-0}(t)+A_{+0}(t)],$$
$$D_y^\dagger(t)=id[A_{-0}(t)-A_{+0}(t)] \tag{13}$$

are the components of the atomic polarization along $\mathbf{e}_x$ and $\mathbf{e}_y$, respectively. Then,

$$G_{\mathbf{n}}(\omega)=(n_y^2+n_z^2)G_X(\omega)+(n_x^2+n_z^2)G_Y(\omega)-n_xn_yG_{XY}(\omega), \tag{14}$$

where

$$G_X(\omega)=\mathrm{Re}\int_0^\infty\langle D_y^\dagger(\tau)D_y(0)\rangle e^{-i\omega\tau}d\tau,$$

$$G_Y(\omega)=\mathrm{Re}\int_0^\infty\langle D_x^\dagger(\tau)D_x(0)\rangle e^{-i\omega\tau}d\tau,$$

$$G_{XY}(\omega)=\mathrm{Re}\int_0^\infty[\langle D_x^\dagger(\tau)D_y(0)\rangle+\langle D_y^\dagger(\tau)D_x(0)\rangle]e^{-i\omega\tau}d\tau. \tag{15}$$

The standard detection arrangements [2,5,6,8], illustrated in Fig. 1(b), measure two basic types of fluorescence spectra, determined by the direction of observation, which we denote $G_X(\omega)$, for detection along the X axis (parallel to the polarization direction of the laser), and $G_Y(\omega)$ for detection along the Y axis (perpendicular to the polarization direction of the laser), respectively. We adopt these arrangements, and consider these quantities in detail. In fact, the single-time correlation functions, $\lim_{t\to\infty}\langle D_x^\dagger(t)D_x(t)\rangle$ and $\lim_{t\to\infty}\langle D_y^\dagger(t)D_y(t)\rangle$, respectively, describe the intensities of the Y polarized and X polarized fluorescence signals of the Hanle effect, and were extensively investigated in the past [2,5,6,8].

The spectra $G_X(\omega)$ and $G_Y(\omega)$ in Eq. (15) are composed of coherent and incoherent components. The coherent Rayleigh parts, whose origin can be traced to the elastic scattering of the driving field, give rise to only δ-function contributions, whilst the incoherent ones, which stem from the fluctuations of the dipole polarizations, make the main contribution. Hereafter we pay attention only to the incoherent Hanle resonance fluorescence spectra, which are defined as

$$G_X^{inc}(\omega)=\mathrm{Re}\int_0^\infty\langle\Delta D_y^\dagger(\tau)\Delta D_y(0)\rangle e^{-i\omega\tau}d\tau,$$

$$G_Y^{inc}(\omega)=\mathrm{Re}\int_0^\infty\langle D_x^\dagger(\tau)\Delta D_x(0)\rangle e^{-i\omega\tau}d\tau, \tag{16}$$

where $\Delta D_l(t)=D_l(t)-\langle D_l(\infty)\rangle$ represents the deviation of the dipole polarization operator $D_l(t)$, $(l=x,y)$, from its mean steady-state value. The two-time correlation functions, $\langle\Delta D_l^\dagger(t)\Delta D_l(0)\rangle$, $(l=x,y)$ can be obtained by invoking the quantum regression theorem [15], together with the optical Bloch equations (3). To do this, we define a vector $\mathbf{U}_l(t)$, $(l=x,y)$ for the steady-state correlations of the atom

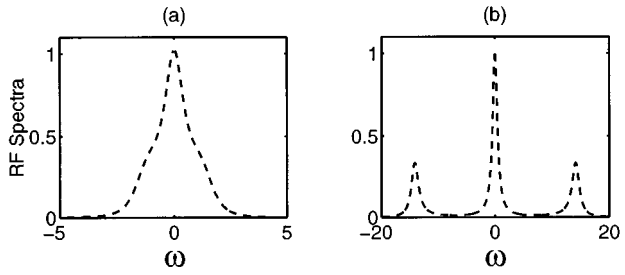

FIG. 2. Incoherent Hanle resonance fluorescence spectra in the absence of a static magnetic field, $\omega_B=0$, and for different Rabi frequencies Ω, (a) $\Omega=0.5$, (b) $\Omega=5$. In all figures, the solid curves denote $G_X^{inc}(\omega)$ (which is zero in the case), whilst the dashed curves represent $G_Y^{inc}(\omega)$. (We take $\gamma=1$ in these graphs.)

$$\mathbf{U}_l(t)=[\langle\Delta A_{+0}(t)\Delta D_l(0)\rangle,\langle\Delta A_{0+}(t)\Delta D_l(0)\rangle,\langle\Delta A_{++}(t)\Delta D_l(0)\rangle,\langle\Delta A_{-0}(t)\Delta D_l(0)\rangle,\langle\Delta A_{0-}(t)\Delta D_l(0)\rangle,\langle\Delta A_{--}(t)\Delta D_l(0)\rangle,\langle\Delta A_{+-}(t)\Delta D_l(0)\rangle,\langle\Delta A_{-+}(t)\Delta D_l(0)\rangle]^T. \tag{17}$$

According to the quantum regression theorem, when $t>0$ we have

$$\frac{d}{dt}\mathbf{U}_l(t)=\underline{\mathcal{B}}\mathbf{U}_l(t), \quad (l=x,y). \tag{18}$$

Due to the time independence of $\underline{\mathcal{B}}$, Eq. (18) is readily solved. Substituting the solution into Eq. (16) one obtains the incoherent resonance fluorescence spectra, $G_X^{inc}(\omega)$ and $G_Y^{inc}(\omega)$ to be

$$G_X^{inc}(\omega)=\mathrm{Re}\left\{\sum_{j=1}^{8} id[R_{4j}(i\omega)-R_{1j}(i\omega)]U_{yj}(0)\right\},$$

$$G_Y^{inc}(\omega)=\mathrm{Re}\left\{\sum_{j=1}^{8} d[R_{4j}(i\omega)+R_{1j}(i\omega)]U_{xj}(0)\right\}, \tag{19}$$

where $U_{xj}(0)$ and $U_{yj}(0)$ are the initial components of the vector $\mathbf{U}_l(t)$, $(l=x,y)$, defined in Eq. (17). $R_{ij}(i\omega)$ is an element of the matrix $\underline{\mathcal{R}}(i\omega)=(i\omega\underline{I}-\underline{\mathcal{B}})^{-1}$ with $\underline{I}$ being the identity matrix.

We show the numerical results of the Hanle fluorescence spectra in the case of $\delta=0$. First of all, we consider the Hanle fluorescence spectra in the absence of an applied magnetic field in Fig. 2. One may, perhaps, expect that this system will possess the same spectral features as that of a two-level atom driven by the same field. However, our results show substantial differences. In the Hanle system, the spectrum is very sensitive to the observed direction. For the experimental geometry [5,6,8] used here, the incoherent fluorescence spectrum, $G_X^{inc}(\omega)$, detected along the X axis (parallel to the polarization direction of the linearly polarized laser field) is null for all driving intensities, whilst the spectrum, $G_Y^{inc}(\omega)$, detected along the Y axis (perpendicular to the polarization direction of the driving laser) exhibits similar structures to that of the Mollow system. For example, in frame 2(a), the spectrum $G_Y^{inc}(\omega)$ consists of a single peak at line center and the sidebands are beginning to grow but are not yet resolved for this weak driving intensity ($\Omega=0.5$), while a Mollow-like triplet is displayed for a large Rabi frequency $\Omega=5$ in frame 2(b). (We measure all frequencies in units of γ.) However, the dressed state analysis presented in Sec. IV shows that the sidebands are shifted by an amount $2\Omega_R=2\sqrt{\omega_B^2+2\Omega^2}=14.4$ from line center, which differs considerably from the value $\Omega=5$ obtained in the resonance fluorescence spectrum of a driven two-level atom [16].

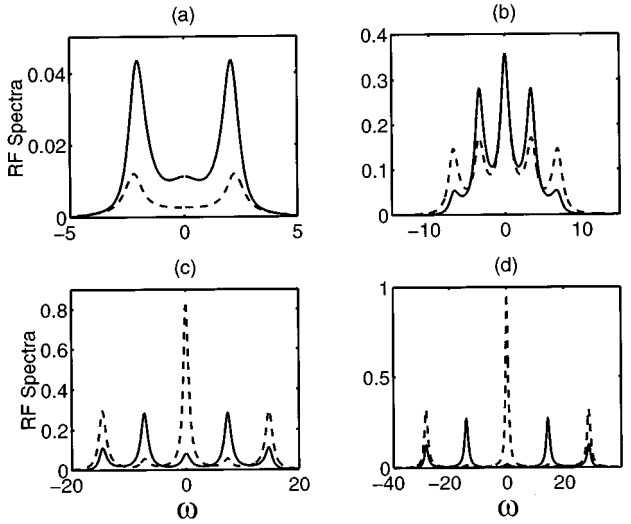

FIG. 3. Same as Fig. 2, but for $\omega_B=2$, and various Rabi frequencies, (a) $\Omega=0.5$, (b) $\Omega=2$, (c) $\Omega=5$, and (d) $\Omega=10$. $G_X^{inc}(\omega)$ in the frames (c) and (d) are multiplied by the factors 5 and 20, respectively, in order to be made visible.

The remarkable directional properties of the spectrum are a direct signature of level crossing and quantum interference effects. For vanishing magnetic fields, $\omega_B=0$, the excited sublevels overlap completely. The coherence produced during optical excitation is conserved and the reemitted radiation shows an angular distribution due to the linearly polarized excitation. Along the polarization direction of the laser the reemitted radiation interferes destructively with the consequence that $G_X^{inc}(\omega)=0$, while the interference in the direction perpendicular to the polarization vector is constructive.

However, if a very weak magnetic field is applied, numerical calculations demonstrate that both resonance fluorescence spectra are qualitatively similar, and display a single peak for small Rabi frequencies. These spectra are not of particular interest and are not shown here.

We have plotted both spectra for the case of $\omega_B=2$ and different excitation intensities Ω in Fig. 3, and for $\Omega=5$ and various magnetic-field intensities in Fig. 4. The spectra have a maximum of five resolved components and are symmetrical. Some spectral lines can be completely suppressed for certain situations. They have the following general properties. When $\omega_B<\Omega$ the central component of the spectrum $G_X^{inc}(\omega)$ is less than that of the spectrum $G_Y^{inc}(\omega)$. When $\omega_B=\Omega$ both spectra have a similar structure and they have the same value at line center. However, when $\omega_B>\Omega$ the central component of $G_X^{inc}(\omega)$ is larger than that of $G_Y^{inc}(\omega)$.

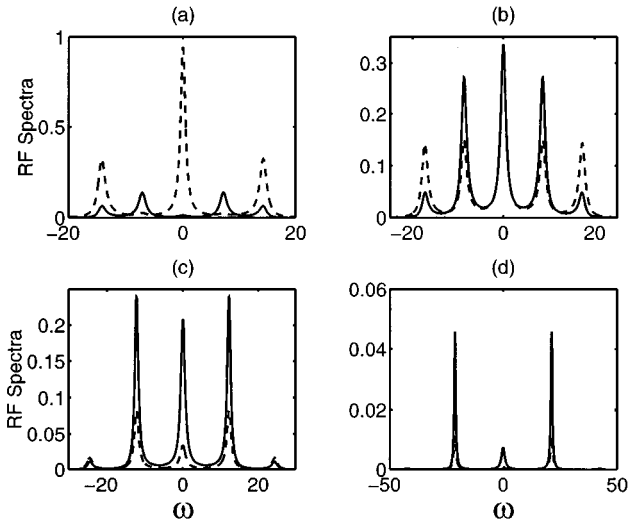

FIG. 4. Same as Fig. 2, but for $\Omega=5$, and different magnetic-field intensities, (a) $\omega_B=1$, (b) $\omega_B=5$, (c) $\omega_B=10$, and (d) $\omega_B=20$. $G_X^{inc}(\omega)$ in frame (a) is multiplied by the factor 10 in order to be made visible.

In the limit of $\omega_B \ll \Omega$, the spectrum, $G_Y^{inc}(\omega)$ has a three-peaked structure similar to that of the Mollow spectrum, whilst the spectrum, $G_X^{inc}(\omega)$, has four peaks. In the limit of $\omega_B \gg \Omega$, both spectra, $G_X^{inc}(\omega)$ and $G_Y^{inc}(\omega)$, have a two-peaked structure similar to that of a two-level atom far off resonance. The directional properties of the spectra are therefore more significant in the limit $\omega_B \ll \Omega$. On the other hand, the integrated areas under the spectral curves, i.e., the fluorescence intensities, are approximately same when $\omega_B=\Omega$, whilst the area under the spectrum $G_X^{inc}(\omega)$ is much greater than that under $G_Y^{inc}(\omega)$ when $\omega_B \gg \Omega$, and vice versa.

IV. DRESSED STATE ANALYSIS

The dressed atomic state representation has proved to be a natural description of the system dynamics which makes the underlying physical processes transparent. In this representation, within the secular approximation, the resonance fluorescence spectra can be expressed in analytical form [17]. In this section we derive explicit expressions for the line shapes, linewidths, and peak heights of the Hanle fluorescence spectra in the dressed state representation in the limit of large effective Rabi frequencies. For simplicity, we here assume that the excitation field is tuned to resonance with the atom, $\delta=0$. In this situation, the eigenvalues and eigenstates of the interaction Hamiltonian (1) are given by

$$\lambda_a=0, \quad \lambda_b=\Omega_R, \quad \lambda_c=-\Omega_R, \tag{20}$$

and

$$|a\rangle=\frac{1}{\eta}[(-|+\rangle+|-\rangle)e^{i\phi_L}+\eta_z|0\rangle],$$

$$|b\rangle=\frac{1}{\eta}[(G_-|+\rangle+G_+|-\rangle)e^{i\phi_L}+|0\rangle],$$

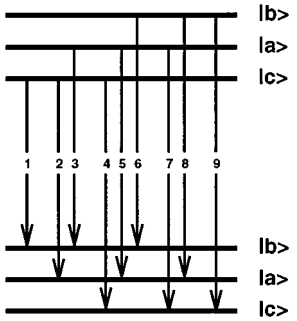

FIG. 5. Level diagram of the dressed atomic states and relevant transitions.

$$|c\rangle=\frac{1}{\eta}[(G_+|+\rangle+G_-|-\rangle)e^{i\phi_L}-|0\rangle], \tag{21}$$

where

$$\Omega_R=\sqrt{\omega_B+2|\Omega|^2}, \quad \eta=\frac{\Omega_R}{|\Omega|}, \quad \eta_z=\frac{\omega_B}{|\Omega|}, \quad G_\pm=\frac{1}{\eta\pm\eta_z}. \tag{22}$$

The energy diagram of the dressed states and the relevant transition processes, which contribute to different spectral lines, are shown in Fig. 5. In the dressed state representation, the underlying physical processes are evident. The equations for the diagonal elements, $\langle\Pi_{aa}\rangle$, $\langle\Pi_{bb}\rangle$, and $\langle\Pi_{cc}\rangle$, are always associated with zero frequency, which reflects the transitions between the same dressed levels, for instance, lines 4, 5, and 6 in Fig. 5. However, the equations of motion of the off-diagonal elements, such as $\langle\Pi_{ac}\rangle$ and $\langle\Pi_{ba}\rangle$ representing transitions 2 and 3, are associated with the effective Rabi frequency Ω_R, whilst $\langle\Pi_{ca}\rangle$ and $\langle\Pi_{ab}\rangle$, representing transitions 7 and 8, are associated with the frequency $-\Omega_R$, and $\langle\Pi_{cb}\rangle$ and $\langle\Pi_{bc}\rangle$ are associated with the frequencies $2\Omega_R$ and $-2\Omega_R$, corresponding to lines 9 and 1, respectively.

In the high-field limit, where the effective Rabi frequency is much greater than all relaxation rates, i.e., $\Omega_R \gg \gamma$, the coupling between matrix elements associated with various frequencies may be omitted to order $O(\omega/\Omega_R)$. Correspondingly, the optical Bloch equations in the dressed state representation are obtained as

$$\langle\dot{\Pi}_{bb}\rangle=-\Gamma_0\langle\Pi_{bb}\rangle+\Gamma_1\langle\Pi_{aa}\rangle+\Gamma_2\langle\Pi_{cc}\rangle,$$

$$\langle\dot{\Pi}_{cc}\rangle=-\Gamma_0\langle\Pi_{cc}\rangle+\Gamma_1\langle\Pi_{aa}\rangle+\Gamma_2\langle\Pi_{bb}\rangle,$$

$$\langle\dot{\Pi}_{ba}\rangle=-(\Gamma_3+i\Omega_R)\langle\Pi_{ba}\rangle+\Gamma_4\langle\Pi_{ac}\rangle,$$

$$\langle\dot{\Pi}_{ca}\rangle=-(\Gamma_3-i\Omega_R)\langle\Pi_{ca}\rangle+\Gamma_4\langle\Pi_{ab}\rangle,$$

$$\langle\dot{\Pi}_{cb}\rangle=-(\Gamma_5+i2\Omega_R)\langle\Pi_{cb}\rangle, \tag{23}$$

with

$$\Gamma_0=\frac{\gamma}{\eta^4}(1+\eta_z^2)^2,$$

$$\Gamma_1=\frac{2\gamma}{\eta^4},$$

$$\Gamma_2=\frac{\gamma}{\eta^4}(1+\eta_z^2),$$

$$\Gamma_3=\frac{\gamma}{\eta^4}\left[\eta_z^2+\frac{1}{2}\eta^2(1+\eta^2)\right],$$

$$\Gamma_4=\frac{\gamma}{\eta^4}\eta_z^2,$$

$$\Gamma_5=\frac{\gamma}{\eta^4}[1+\eta^2(1+\eta_z^2)]. \tag{24}$$

Only the diagonal elements are nonzero in the steady state

$$\langle\Pi_{bb}\rangle=\langle\Pi_{cc}\rangle=\frac{2}{4+\eta_z^2(1+\eta_z^2)},$$

$$\langle\Pi_{aa}\rangle=\frac{\eta_z^2(1+\eta_z^2)}{4+\eta_z^2(1+\eta_z^2)}. \tag{25}$$

Employing the quantum regression theorem [15], we can express the resonance fluorescence spectra $G_X^{inc}(\omega)$ and $G_Y^{inc}(\omega)$ in the transparent forms

$$G_X^{inc}(\omega)=\mathrm{Re}\left[\frac{\sigma_0}{i\omega+\Gamma_0+2\Gamma_1-\Gamma_2}+\frac{\sigma_1}{i\omega+i\Omega_R+\Gamma_3-\Gamma_4}+\frac{\sigma_2}{i\omega+i\Omega_R+\Gamma_3+\Gamma_4}+\frac{\sigma_3}{i\omega-i\Omega_R+\Gamma_3-\Gamma_4}+\frac{\sigma_4}{i\omega-i\Omega_R+\Gamma_3+\Gamma_4}+\frac{\sigma_5}{i\omega-i2\Omega_R+\Gamma_5}+\frac{\sigma_6}{i\omega+i2\Omega_R+\Gamma_5}\right], \tag{26}$$

where

$$\sigma_0=\frac{9\eta_z^2}{\eta^4}\langle\Pi_{aa}\rangle(\langle\Pi_{bb}\rangle+\langle\Pi_{cc}\rangle),$$

$$\sigma_1=\frac{1}{2\eta^2}(\eta_z^2\langle\Pi_{bb}\rangle+2\langle\Pi_{aa}\rangle),$$

$$\sigma_2=\frac{\eta_z^2-2}{2\eta^4}(\eta_z^2\langle\Pi_{bb}\rangle-2\langle\Pi_{aa}\rangle),$$

$$\sigma_3=\frac{1}{2\eta^2}(\eta_z^2\langle\Pi_{cc}\rangle+2\langle\Pi_{aa}\rangle),$$

$$\sigma_4=\frac{\eta_z^2-2}{2\eta^4}(\eta_z^2\langle\Pi_{cc}\rangle-2\langle\Pi_{aa}\rangle),$$

$$\sigma_5=\frac{\eta_z^2}{\eta^4}\langle\Pi_{bb}\rangle,$$

$$\sigma_6=\frac{\eta_z^2}{\eta^4}\langle\Pi_{cc}\rangle. \tag{27}$$

The incoherent Hanle fluorescence spectrum, $G_X^{inc}(\omega)$, consists of five spectral components: the central line with width $2(\Gamma_0+2\Gamma_1-\Gamma_2)$, the outer sidebands located at frequencies $\pm2\Omega_R$ with widths of $2\Gamma_5$, and the inner sidebands, placed at frequencies $\pm\Omega_R$, which, however, are a superposition of two Lorentzians with widths $2(\Gamma_3\pm\Gamma_4)$. The heights of these peaks are proportional to the given parameters σ_i. The heights of the central peak, and of the inner and the outer sidebands, are given, respectively, by

$$P_x(0)=\frac{\sigma_0}{\Gamma_0+2\Gamma_1-\Gamma_2},$$

$$P_x(\pm\Omega_R)=\frac{\sigma_1}{\Gamma_3-\Gamma_4}+\frac{\sigma_2}{\Gamma_3+\Gamma_4},$$

$$P_x(\pm2\Omega_R)=\frac{\sigma_5}{\Gamma_5}. \tag{28}$$

Also

$$G_Y^{inc}(\omega)=\mathrm{Re}\left[\frac{\epsilon_0}{i\omega+\Gamma_0+\Gamma_2}+\frac{\epsilon_1(i\omega+i\Omega_R+\Gamma_3)}{(i\omega+i\Omega_R+\Gamma_3)^2-\Gamma_4^2}+\frac{\epsilon_2(i\omega-i\Omega_R+\Gamma_3)}{(i\omega-i\Omega_R+\Gamma_3)^2-\Gamma_4^2}+\frac{\epsilon_3}{i\omega-i2\Omega_R+\Gamma_5}+\frac{\epsilon_4}{i\omega+i2\Omega_R+\Gamma_5}\right] \tag{29}$$

where

$$\epsilon_0=\frac{1}{\eta^2}(\langle\Pi_{bb}\rangle+\langle\Pi_{cc}\rangle),$$

$$\epsilon_1=\frac{\eta_z^2}{\eta^2}\langle\Pi_{bb}\rangle,$$

$$\epsilon_2=\frac{\eta_z^2}{\eta^2}\langle\Pi_{cc}\rangle,$$

$$\epsilon_3=\frac{1}{\eta^2}\langle\Pi_{bb}\rangle,$$

$$\epsilon_4=\frac{1}{\eta^2}\langle\Pi_{cc}\rangle. \tag{30}$$

The incoherent resonance fluorescence spectrum $G_Y^{inc}(\omega)$ also has five contributions. One is centered at the transition frequency ω_A, two sidebands are displaced by an amount $\pm\Omega_R$ from the central line, and there are two additional Lorentzians with the same width $2\Gamma_5$ displaced by $\pm2\Omega_R$ from the central peak. The heights of the spectral components are given by

$$P_y(0)=\frac{\epsilon_0}{\Gamma_0+\Gamma_2},\tag{31}$$

$$P_y(\pm\Omega_R)=\frac{\epsilon_1\Gamma_3}{\Gamma_3^2-\Gamma_4^2},$$

$$P_y(\pm 2\Omega_R)=\frac{\epsilon_3}{\Gamma_5}.$$

Various components of both spectra $G_X^{inc}(\omega)$ and $G_Y^{inc}(\omega)$ are associated with different transitions in the dressed states. The central peak is related to transitions between the same dressed levels, and the outer sidebands originate from transitions between the dressed states $|b\rangle$ and $|c\rangle$. However, other transitions contribute to the inner sidebands. From the equations of motion (23) in the dressed state representation, we find that the transitions between $|b\rangle\leftrightarrow|a\rangle$ and $|a\rangle\leftrightarrow|c\rangle$ are entangled, so that the inner peaks have a complicated structure. The inner sidebands in the spectrum $G_X^{inc}(\omega)$ are superpositions of two Lorentzians with different heights and widths, whilst the inner sidebands of $G_Y^{inc}(\omega)$ take a complicated, non-Lorentzian shape.

On the other hand, as the stationary dressed state populations $\langle\Pi_{bb}\rangle$ and $\langle\Pi_{cc}\rangle$ are identical in the secular approximation, both inner peaks have the same shape, and the pair of outer sidebands also have the same height and width.

Furthermore, we may consider certain special situations. (i) Without the magnetic field, $\omega_B=0$, the upper level is degenerate. In this case, $\eta_z=0$, $\eta=\sqrt{2}$, and the steady-state populations of the dressed states reduce to $\langle\Pi_{bb}\rangle=\langle\Pi_{cc}\rangle=\frac{1}{2}$ and $\langle\Pi_{aa}\rangle=0$, which demonstrates that the atom is trapped in a superposition of the dressed states $|b\rangle$ and $|c\rangle$. The resultant spectrum $G_X^{inc}(\omega)=0$. However, for the spectrum $G_Y^{inc}(\omega)$, only the inner sidebands disappear, giving a triplet structure of the form

$$G_Y^{inc}(\omega)=\frac{1}{2}\langle\Pi_{bb}\rangle\left[\frac{2(\Gamma_0+\Gamma_2)}{(\Gamma_0+\Gamma_2)^2+\omega^2}+\frac{\Gamma_5}{\Gamma_5^2+(\omega+2\Omega_R)^2}+\frac{\Gamma_5}{\Gamma_5^2+(\omega-2\Omega_R)^2}\right],$$

which resembles the Mollow spectrum of a two-level atom. It is not difficult to see that the ratios of the height and width of the central peaks to those of the sidebands are 3 and 2/3, respectively, the same as in the Mollow triplet [16]. However, the sidebands are displaced by $2\Omega_R$ from line center, instead of Ω_R as in the original Mollow case. See Fig. 2(b). The absolute widths of the peaks also differ from the Mollow values. (ii) $\omega_B\neq 0$, but $\omega_B\ll\Omega$, so that $\eta_z\ll 1$, $\eta_\lambda\simeq\sqrt{2}$. The resultant resonance fluorescence spectra, $G_X^{inc}(\omega)$ and $G_Y^{inc}(\omega)$ exhibit a five-peak structure. Furthermore, through analyzing the parameters σ_l, $(l=0,1,\ldots,6)$ and ϵ_k, $(k=0,1,\ldots,4)$ we find that (a): $\sigma_0,\sigma_5,\sigma_6\ll\sigma_1,\sigma_2,\sigma_3,\sigma_4$, which implies that the heights of the inner sideband peaks are much larger than those of the central peak and outer sidebands in the spectrum $G_X^{inc}(\omega)$; and (b): $\epsilon_0,\epsilon_3,\epsilon_4,\gg\epsilon_1,\epsilon_2$, which means that the inner sideband height is very small: $G_Y^{inc}(\omega)$ is a triplet. These conclusions are in excellent agreement with Figs. 3(c), 3(d), and 4(a). (iii) $\omega_B=\Omega\gg\gamma$, so that $\eta_z=1$, $\eta=\sqrt{3}$. In this case, the populations of the dressed states are identical, $\langle\Pi_{aa}\rangle=\langle\Pi_{bb}\rangle=\langle\Pi_{cc}\rangle=1/3$, and from Eq. (27), we have $\sigma_0=2/9$, $\sigma_1=\sigma_3=1/6$, $\sigma_2=\sigma_4=1/54$, $\sigma_5=\sigma_6=1/27$. Therefore, the heights of the five peaks of the spectrum $G_X^{inc}(\omega)$ are given by

$$P_x(0)=\tfrac{1}{3},$$

$$P_x(\pm\Omega_R)=\tfrac{13}{48},$$

$$P_x(\pm 2\Omega_R)=\tfrac{1}{21}.\tag{32}$$

In general, the height of the central component is a little larger than that of the inner sidebands which in turn are larger than that of the outer ones. See Figs. 3(b) and 4(b).

On the other hand, from Eq. (30), we have $\epsilon_0=2/9$, $\epsilon_1=\epsilon_2=\epsilon_3=\epsilon_4=1/9$. Correspondingly, the peak heights of the spectrum $G_Y^{inc}(\omega)$ are reduced to

$$P_y(0)=\tfrac{1}{3},$$

$$P_y(\pm\Omega_R)=\tfrac{7}{48},$$

$$P_y(\pm 2\Omega_R)=\tfrac{1}{7}.\tag{33}$$

The central height is larger than that of the inner pair which is approximately equal to that of the outer pair. For instance, see frames 3(b) and 4(b).

Comparing Eq. (32) with Eq. (33) shows that the central heights of both spectra are the same, see Figs. 3(b) and 4(b). (iv)$\omega_B\gg\Omega$. We then have $\eta_z\simeq\eta\gg 1$, and the populations $\langle\Pi_{bb}\rangle=\langle\Pi_{cc}\rangle$ are very small, while $\langle\Pi_{aa}\rangle$ is close to 1. From Eq. (27) one gets

$$\sigma_0=\frac{9}{\eta^2}\langle\Pi_{aa}\rangle(\langle\Pi_{bb}\rangle+\langle\Pi_{cc}\rangle),$$

$$\sigma_1=\sigma_3=\tfrac{1}{2}\langle\Pi_{bb}\rangle+\frac{1}{\eta^2}\langle\Pi_{aa}\rangle,$$

$$\sigma_2=\sigma_4=\tfrac{1}{2}\langle\Pi_{bb}\rangle-\frac{1}{\eta^2}(\langle\Pi_{aa}\rangle+\langle\Pi_{bb}\rangle),$$

$$\sigma_5=\sigma_6=\frac{1}{\eta^2}\langle\Pi_{bb}\rangle.\tag{34}$$

Due to η^{-2} being very small, only the inner sideband is dominant, and the other peaks are too small to be visible in the spectrum $G_X^{inc}(\omega)$. See Figs. 3(a) and 4(d).

On the other hand, from Eq. (30) we have

$$\epsilon_0=\frac{2}{\eta^2}\langle\Pi_{bb}\rangle,$$

$$\epsilon_1=\epsilon_2=\langle\Pi_{bb}\rangle,$$

$$\epsilon_3=\epsilon_4=\frac{1}{\eta^2}\langle\Pi_{bb}\rangle.\tag{35}$$

As in the spectrum $G_X^{inc}(\omega)$, only the inner sidebands are visible, and the others almost disappear. We also find that both spectra have qualitatively similar structure, but with different heights when $\omega_B \gg \Omega$.

V. SUMMARY

In this paper we have investigated the directional properties of the steady-state incoherent resonance fluorescence spectra of the Hanle effect in a V-type atom with a $J_g=0 \leftrightarrow J_e=1$ transition, excited by a linearly polarized laser. There exist two principal types of Hanle spectra, which are differentiated by the direction of observation.

In the case of $\omega_B=0$ (no magnetic field), the incoherent spectrum $G_X^{inc}(\omega)$, detected along the polarization direction of the excitation field, is zero all excitation intensities, whereas the spectrum $G_Y^{inc}(\omega)$, detected along the direction perpendicular to the polarization direction of the laser, exhibits a single peak at weak laser intensities, and at high excitation intensities, a Mollow-like triplet but with sideband shifts $2\Omega_R$, instead of Ω_R, the effective Rabi frequency in the original Mollow case [16]. However, if a magnetic field is applied ($\omega_B \neq 0$), the incoherent spectra are composed in general of five peaks. When $\omega_B < \Omega$, the amplitude of the central peak in the spectrum $G_X^{inc}(\omega)$ is less than that of $G_Y^{inc}(\omega)$; and vice versa when $\omega_B > \Omega$. Both central peaks have the same height and the integrated areas under both spectra are also approximately equal when $\omega_B=\Omega$. Some peaks can be suppressed for certain choices of the parameters. For example, in the limit of $\omega_B \ll \Omega$, the incoherent spectrum $G_X^{inc}(\omega)$ has four peaks, whilst $G_Y^{inc}(\omega)$ has a Mollow-like triplet with sideband shifts $2\Omega_R$, and the integrated area under the spectrum $G_X^{inc}(\omega)$ is much less than that of $G_Y^{inc}(\omega)$. When $\omega_B \gg \Omega$, both incoherent spectra have a two-peaked structure similar to that of a two-level atom far off resonance, but the integrated area of the spectrum $G_X^{inc}(\omega)$ is much greater than that of $G_Y^{inc}(\omega)$. The directional properties of the resonance fluorescence spectra are more marked when $\omega_B \ll \Omega$, when the destructive interference in the angular distribution of atomic radiation from the excited sublevels dominates.

These results obtained are interpreted in the dressed atomic state representation. Under the secular approximation, we have derived compact expression for the resonance fluorescence spectra which allow us to interpret the spectra in a simple way. The analytical calculations are in excellent agreement with the exact numerical results.

It is worth noting that the Hanle effect has been extensively investigated experimentally [1,3,5]. Therefore, experiments on the Hanle fluorescence spectra studied here, which demonstrate interesting directional properties arising from quantum interference effects, are feasible.

ACKNOWLEDGMENTS

This work is supported by the United Kingdom EPSRC, the EC, and by a NATO Collaborative Research Grant P.Z. wishes to thank the Queen's University of Belfast for financial support.

[1] W. Hanle, Z. Phys. **30**, 93 (1924); A. Corney, *Atomic and Laser Spectroscopy* (Oxford University Press, London, 1977).
[2] P. Avan and C. Cohen-Tannoudji, J. Phys. (Paris) **36**, L85 (1975).
[3] W. Rasmussen, R. Schieder, and H. Walther, Opt. Commun. **12**, 315 (1974); J. D. Cresser, J. Hager, G. Leuchs, M. Rateike, and H. Walther, in *Dissipative System in Quantum Optics*, edited by R. Bonifacio (Springer, Berlin, 1982).
[4] P. Avan and C. Cohen-Tannoudji, J. Phys. B **10**, 171 (1977).
[5] K. Arnett, S. J. Smith, R. E. Ryan, T. Bergeman, H. Metcalf, M. W. Hamilton, and J. R. Brandenberger, Phys. Rev. A **41**, 2580 (1990).
[6] R. E. Ryan and T. H. Bergeman, Phys. Rev. A **43**, 6142 (1991).
[7] S. Dixit, P. Zoller, and P. Lambropoulos, Phys. Rev. A **21**, 1289 (1980).
[8] P. Zhou and S. Swain, Opt. Commun. **123**, 297 (1996).
[9] G. S. Agarwal, C. V. Kunasz, and J. Cooper, Phys. Rev. A **36**, 5654 (1987).
[10] P. A. Lakshmi and G. S. Agarwal, Phys. Rev. A **32**, 1643 (1985).
[11] R. Kaiser, N. Vansteenkiste, A. Aspect, E. Arimondo, and C. Cohen-Tannoudji, Z. Phys. D **18**, 17 (1991).
[12] Z. Phys. D **18** (1) (1991), special issue on level crossing, and references therein.
[13] A. A. Panteleev and F. A. Lomaya, J. Opt. Soc. Am. B **11**, 1153 (1994).
[14] J. N. Dodd, *Atoms and Light Interactions* (Plenum, New York, 1991).
[15] M. Lax, Phys. Rev. **172**, 350 (1968); S. Swain, J. Phys. A **14**, 2577 (1981).
[16] B. R. Mollow, Phys. Rev. **188**, 1969 (1969).
[17] C. Cohen-Tannoudji and S. Reynaud, J. Phys. B **10**, 345 (1977); T. A. B. Kennedy and S. Swain, Phys. Rev. A **36**, 1747 (1987); L. M. Narducci, M. O. Scully, G. L. Oppo, P. Ru, and J. R. Tredicci, *ibid*. **42**, 1630 (1990).